Composites Science and Technology 184 (2019) 107836

Contents lists available at ScienceDirect

Composites Science and Technology

journal homepage: http://www.elsevier.com/locate/compscitech

Improvement of physical and mechanical properties on bio-polymer matrix composites using morphed graphene

O. Velazquez-Meraz [a,b,1], J.E. Ledezma-Sillas [a,1], C. Carreño-Gallardo [a,1], W. Yang [c,1], N. M. Chaudhari [c,1], H.A. Calderon [d], I. Rusakova [e], F.C. Robles Hernandez [b,c,f,*], J. M. Herrera-Ramirez [a,b,**]

[a] Centro de Investigacion en Materiales Avanzados (CIMAV), Laboratorio Nacional de Nanotecnologia, Miguel de Cervantes 120, 31136, Chihuahua, Chih, Mexico
[b] Department of Mechanical Eng. Technology, University of Houston, Houston, TX, USA
[c] Department of Materials Science and Eng., University of Houston, Houston, TX, USA
[d] Instituto Politécnico Nacional, Departamento de Física, ESFM-IPN, UPALM Ed. 9, Mexico CDMX 07738, Mexico
[e] Texas Center for Super Conductivity, University of Houston, Houston, TX, USA
[f] Department of Electrical and Computer Eng., University of Houston, Houston, TX, USA

A B S T R A C T

Chitosan is a natural-occurring biopolymer found commonly in the exoskeleton of crustaceans, vegetables, fungi and plants. Due to its relatively high mechanical properties, chitosan, is attractive for structural applications. Here, we show the benefits of morphed graphene as reinforcement for chitosan composites. Morphed graphene is incorporated into the chitosan matrix via thermomechanical process to produce composites with tunable mechanical performances that are ideal for applications where impact resistant (toughness) and elasticity are required. Optimum sintering conditions were determined by means of thermogravimetry and calorimetry. The characterization results show a clear homogeneity of the microstructure between chitosan and the reinforcement material. The characterization of the composite was carried using X-ray diffraction (XRD), Raman and infrared spectroscopies, optical microscopy, scanning and transmission electron microscopy. The mechanical properties were evaluated by nanoindentation and microhardness tests. The composite sintered at 180 °C for 3 h with 5 wt% of morphed graphene demonstrated to provide the best performance with 33% higher density, 78% less porosity, 133% higher maximum penetration depth, 25% superior hardness, and 73% higher elastic energy ratio. The combination of the reinforcement, morphed graphene, and the technology presented herein are ideal to produced fully dispersed/highly homogeneous composites with up to 5 wt% C. Therefore, morphed graphene additions have unique benefits as chitosan reinforcement material can be used for structural applications such as packaging with environmental advantages over polymers such as Polyethylene Terephthalate. The manufacturing methodology has potential for industrial scalability and presumably the composite is recyclable and compostable.

1. Introduction

Chitosan is a polysaccharide obtained by deacetylating chitin, which is the major constituent of the exoskeleton of crustaceous water animals [1], vegetables and plants [2,3]. Chitin is the second most abundant natural polymer, after the cellulose. The main sources are invertebrate animals (insects and crustaceans) and some fungi [4,5]. There is a wide variety of carbon nanostructures (CNS) that are mainly sp2 bonded such as graphene, carbon nanotubes and fullerenes [6–9]. More recently, we proposed the existence of an outstanding carbon nanostructure known as morphed graphene with a wide range of applications and here we present its potential as a reinforcement for structural bio-materials [10–12]. The goal in polymer composites is to increase their multi-functional character by adding a reinforcement having high aspect ratio and extraordinary mechanical strength [13]. Morphed graphene is selected for the present work due to its unique elastic behavior, versatility, percolation potential and its rather simple processing methods for composite manufacturing including mechanical milling and conventional sintering [7,14–19].

In this work, we demonstrate the potential of morphed graphene to reinforce biopolymers such as chitosan [20–22] to improve its mechanical properties. Ideally, the goal of this work is to use this composite for food packaging or as mechanically robust implantable scaffolds for tissue regeneration, where improved toughness is required. The

* Corresponding author. Department of Mechanical Eng. Technology, University of Houston, Houston, TX, USA.
** Corresponding author. Centro de Investigacion en Materiales Avanzados (CIMAV), Laboratorio Nacional de Nanotecnologia, Miguel de Cervantes 120, 31136, Chihuahua, Chih, Mexico.
E-mail addresses: fcrobles@uh.edu (F.C. Robles Hernandez), martin.herrera@cimav.edu.mx (J.M. Herrera-Ramirez).
[1] Authors with similar contribution.

https://doi.org/10.1016/j.compscitech.2019.107836
Received 14 March 2019; Received in revised form 21 September 2019; Accepted 25 September 2019
Available online 26 September 2019

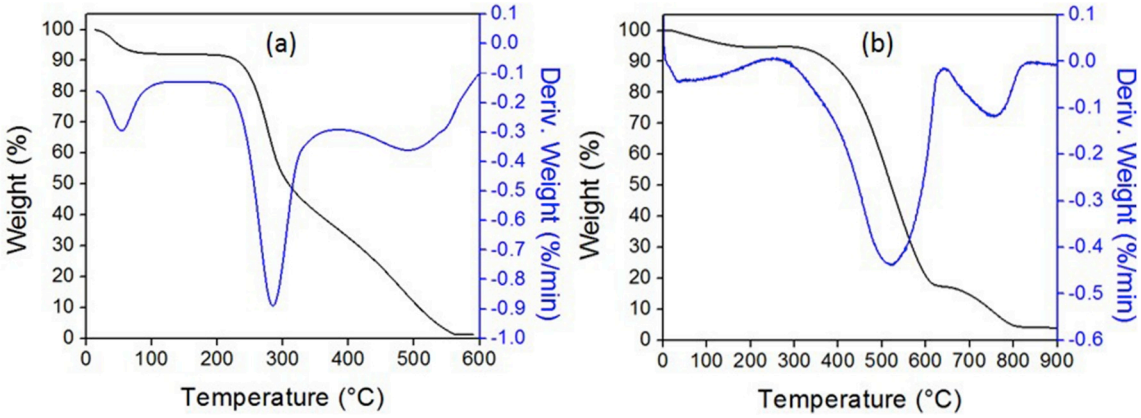

Fig. 1. TGA/DSC curves of (a) chitosan and (b) raw carbon.

morphed graphenes can be synthesized in-situ and they are responsible for the evolution of the outstanding properties (e.g. elastic behavior, hardness, stiffness, etc.) on the final composite. The characterization in this work was carried by means of TGA/DSC, Raman and infrared spectroscopies, XRD, optical microscopy, SEM and HRTEM, and mechanically tested under nanoindentation and microhardness.

2. Methods

Samples were prepared using low (50–190 kDa) molecular weight chitosan powder (Sigma-Aldrich®, St. Louis MO) with a deacetylation degree of 80% and morphed graphenes were prepared as per [10,11]. Mechanical milling was conducted on a high-energy Spex mill using stainless steel vial and media. Chitosan was milled for up to 6 h. Chitosan/CNS composite samples were mixed at 99:1, 97:3 and 95:5 wt ratios and milled together for an additional 1.5 h. A ball-to-powder weight ratio of 10:1 was used. The sintering process was performed on a custom-made French press heated by means of a custom made resistance furnace. The temperature was monitored via a high speed, high resolution data acquisition system (NIcDAQ-9174: National Instruments, Austin, TX) coupled to a PC. A K-type thermocouple was used for controlling the temperatures at 120, 150, 180 and 220 °C for 3 and 5 h. These sintering temperatures were proposed as Ts = (0.7–0.8)*Tm [23], where Tm represents the phase transition temperature, or degradation state. All experiments were carried out in a helium atmosphere and under a constant pressure of 3.5 MPa through the entire sintering process. Disk-shaped samples (~30 mm in diameter and ~4 mm in thickness) were obtained.

Thermogravimetric analysis was carried in a DSC Autosampler TA Instruments using 2–3 mg of sample and a heating rate of 5 °C/min in an air atmosphere. X-ray diffraction (XRD) was performed with an X'Pert MPD diffractometer (Cu Kα = 0.15406 nm). Crystallinity index was determinated by the Focher et al. method [24] using the expression: %CI = $[(I_{110}\text{-}I_{am})/I_{110}]$*100, where %CI is the crystallinity index, and I_{110} and I_{am} are the intensities for the reflection (110) for the β-phase and the amorphous phase (α), respectively. Raman analysis was done by a confocal micro-Raman microscope Xplora, Horiba JY with a 638 nm illumination. The Fourier transformed infrared spectroscopy (FTIR) was carried in the region between 500 and 4000 cm^{-1} in a PerkinElmer FTIR. The powdery chitosan was mixed thoroughly with KBr and then, pressed to a homogeneous disk with a thickness of 0.5 mm. Optical microscopy was carried in a Zeiss Axio Scope A1 using polarized light. Scanning electron microscopy analysis was performed using JEOL JSM-7401F and HITACHI SU3500 microscopes operated at 5 kV and 15 kV, respectively. Transmission electron microscopy was carried in a HITACHI HT7700 microscope. Morphed graphene atomic resolution images were made in a TEAM 05 microscope using low dose conditions [10,11].

Hardness and elastic modulus of samples were evaluated at the nanoscale level by nanoindentation tests in an Agilent Technology Nano Indenter G200 coupled with a DCM II head, using the Oliver-Pharr method [25]. Nanoindentation tests were performed in a system with real-time data collection using a Berkovich indenter tip. All the nanoindentation experiments were performed at a maximum load of 0.2 mN; the reported values are the average of four measurements. The energy to elastically and plastically deform the Chitosan/CNS composites was obtained from the area under the load-displacement (P-h) curve, according to Ref. [26]. The elastic energy ratio was determined using the relationship between elastic energy and the total applied energy. At the microscale level, Vickers microhardness was measured in a LECO LM 300 AT Series tester with a load of 200 gf and a dwelling time of 10 s; six measurements were performed in a different zone and the results were averaged. The porosity measurements were made using the method proposed in Ref. [27].

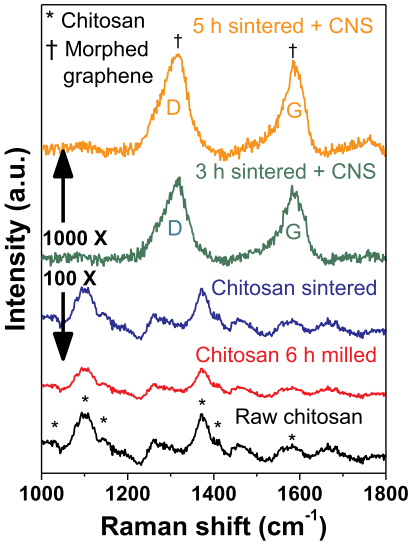

Fig. 2. Raman spectra for chitosan samples and chitosan/CNS composites sintered at 180 °C for 3 and 5 h.

3. Results and discussion

3.1. Thermal analysis

Fig. 1a shows TGA/DSC curves for chitosan, where the first thermal event is observed at 56 °C, which is attributed to the loss of water (8 wt %) weakly bonded to the polymeric structures. The following thermal

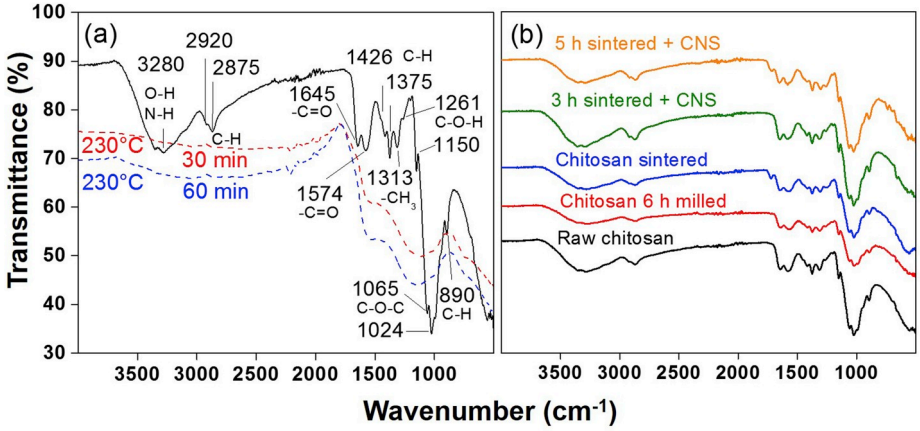

Fig. 3. Infrared spectra of (a) chitosan before and after heating at 230 °C for 30 min and 60 min, and (b) chitosan samples and chitosan/CNS composites sintered at 180 °C for 3 and 5 h.

event takes place at 225 °C and it is attributed to the degradation of the chitosan, including both decomposition and oxidation reactions. In this event the weight loss is approximately 50 wt% and ends at 287 °C, which is attributed to a depolymerization process [28]. Fig. 1b presents the TGA/DSC curve for the raw carbon used to synthesize morphed graphenes demonstrating its stability in air to temperatures of approximately 300 °C. Yet, there is a weight lost (5.3 wt%), potentially due to humidity and organic residue. The weight loss (90.5 wt%) during heating to 900 °C is first due to the oxidation of the amorphous material, followed by oxidation of the short-order graphitic structures and finally morphed graphenes above 615 °C [29].

3.2. Raman spectroscopy

Fig. 2 shows the Raman spectra of the raw, as-milled and as-sintered chitosan samples, as well as the composites (chitosan/morphed graphenes) sintered at 180 °C for 3 and 5 h. These spectra were taken at 100X and 1000X magnifications for chitosan and composite samples, respectively. Under a 100X magnification, Raman active bands of chitosan can be identified by the vibration of the C – O stretch at 1080 and 1030 cm^{-1}, which corresponds to the saccharide structure. The antisymmetric stretches of the C – O – C bridge at 1155 cm^{-1}, C – H bending at approximately 1380 and 1423 cm^{-1} and the N – H bending at 1598 cm^{-1} correspond to the primary amine group [30]. Under a 1000X magnification, the presence of morphed graphene is identified by the D (1318 cm^{-1}) and G (1578 cm^{-1}) bands, demonstrating the graphitic nature of this structure. The higher magnification lets better identification of the morphed graphene, allowing us to conclude that morphed graphenes are found along the surface of chitosan particles that in turn imply improved percolation. This is further confirmed by the black coloration of the composites. The Raman spectra for both sintering times are almost identical to the raw sample, which demonstrates that the chitosan bonding structure is preserved during and after the sintering process.

3.3. Infrared spectroscopy

The FTIR spectra of Fig. 3a shows the characteristic absorption bands of chitosan, which belong to the functional groups: 3750-3000 cm^{-1}, ν(O – H) and νs(N – H); 2920 cm−1, νas(C – H); 2875 cm−1, νs(C – H); 1645 cm−1, ν(– C = O) secondary amide; 1574 cm−1, ν(– C = O) protonated amide; 1426 and 1375 cm−1, δ(C – H); 1313 cm−1, νs(– CH3) tertiary amide; 1261 cm−1, ν(C – O – H); 1150, 1065, and 1024 cm−1, νas(C– O – C) and νs(C– O – C); and 890 cm−1, ω(C – H). After heating above its thermal degradation temperature (230 °C) for 30 min and 60 min in an air atmosphere the spectra show clear changes. The changes are attributed to the polymer degradation that is in agreement with the thermal analysis results. The intensity of the band at 3280 cm^{-1} decreases due to dehydration or the loss of oxhidrile groups. In the case of bands at 1645 and 1580 cm−1 one can observe the loss of the acetyl and amino groups. The bands at 2932, 2867 as well as those found below 1420 cm^{-1} have a drop in intensity that is attributed to depolymerization reactions [31].

All this indicates that sintering above the thermal degradation temperature causes negative effects in the synthesis of the composite. This is mainly due to the loss of the main functional groups of chitosan. Here, we conclude that the sintering temperature for chitosan is key to prevent complete degradation of this material. Therefore, it is needed to

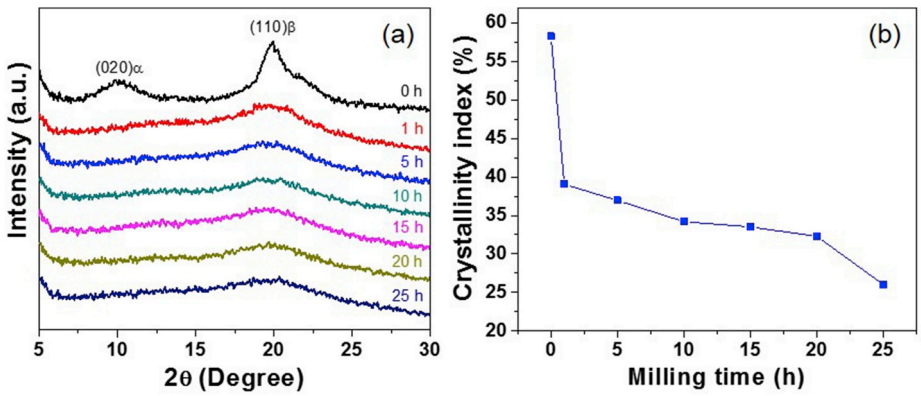

Fig. 4. (a) XRD results and (b) crystallinity index analysis of chitosan at different milling times.

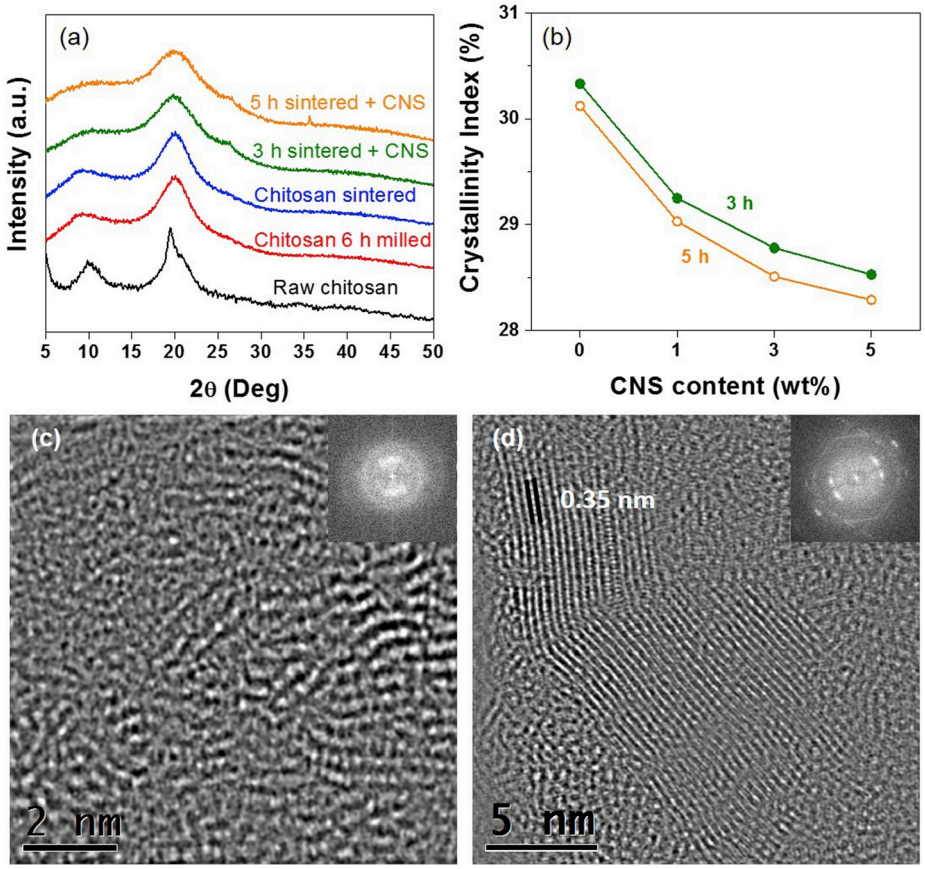

Fig. 5. (a) XRD results for chitosan samples and chitosan/CNS composites sintered at 180 °C for 3 and 5 h. (b) Crystallinity index analysis of these composites. Atomic resolution TEM under low dose method showing (c) the raw carbon (quasi-amorphous) and (d) a particle of morphed graphene. Note: the d-spacing in morphed graphene is between 0.345 and 0.37 nm as compared to that in graphene that is typically 0.33 nm.

complement the Raman results with FTIR and TGA/DSC as possible to truly understand the state of the chitosan molecules before and after sintering. The FTIR also confirms the Raman results where we observe no potential chemical interactions among chitosan and morphed graphenes (Fig. 3b). The structural features of morphed graphenes are clearly identified by their graphitic nature as demonstrated based on the D and G Raman bands. The lack of potential bonding with chitosan is investigated through the hydroxyl, amino and acetyl groups [32]. These spectra reveal that the bonding structure of chitosan is not affected by the presence of carbon or the milling process.

3.4. X-ray diffraction

Fig. 4a shows the XRD patterns of chitosan samples at different milling times. Chitosan has two main characteristic peaks at $2\theta = 10°$ and 20°, which consist of the α-chitin (amorphous) and β-chitin (crystalline) phases, respectively [24]. This means that chitosan has dual phase frameworks and the bulk can be considered semi-crystalline. The α-chitin phase has a structure of antiparallel chains while β-chitosan phase has intrasheet hydrogen-bonding by parallel chains [33]. The XRD results reveal that the intensity of the characteristic peak in β-chitin decreases and become broadened with milling time. This causes a reduction in the crystallinity index (Fig. 4b) due to micro or nano-deformations in the lattice, owing to the high-energy ball milling [34]. In conclusion the optimum milling time is between 5 and 6 h when the crystallinity index is above 35%. Below 35% the composite does not sinter properly due to an excessive deformation in the β-chitin, preventing re-crystallization during sintering and this compromises the mechanical benefits of morphed graphene.

Fig. 5a shows the diffraction patterns of the raw, as-milled and as-sintered chitosan samples, as well as those of the composite samples sintered at 180 °C for 3 and 5 h. The α-chitin and β-chitin phases are present in each diffraction pattern. However, when morphed graphenes are added to the chitosan matrix, the intensity of the characteristic peaks of chitosan decreases and become broadened. The characteristic peak of the (002) plane ($2\theta = \sim 26.3°$) corresponds to graphitic carbon seen in Fig. 5c–d for the raw and milled carbon. Yet, the presence of the morphed graphene is not clear in the milled samples a it blends over the chitosan. It is important to mention that the synthesis of the morphed graphenes is unique and consists on milling of the raw sample at room temperature [10,11].

The crystalline structure of chitosan does not seem to be affected by the presence of morphed graphenes; however, the crystallinity index decreases (Fig. 5b). A potential reason is perhaps the difference in stiffness of the morphed graphene and chitosan. The morphed graphene has a high elastic moduli with the potential to break through the chitosan particles that in a way compromises the chitosan's crystalline structure. This is probably the single most important effect and mechanism observed in the composites as this turns to be the most effective reinforcement effect observed with chitosan. This reinforcement effect anchors the chitosan grains in a unique form enhancing the structural properties and reinforcement in the composite. The morphed graphene behaves like fibers within the chitosan structure improving their mechanical performance, as shown in HRTEM.

The morphed graphene lock or anchors the chitosan particles hindering their mobility that in turn results in an strengthening mechanism that sponsors hardness, strength, stiffness and the toughness improvements in the composite. Similar behavior has been previously reported [35]. As the sintering time increases the integration of the morphed graphene increases potentially due to a relaxation (e.g. annealing or

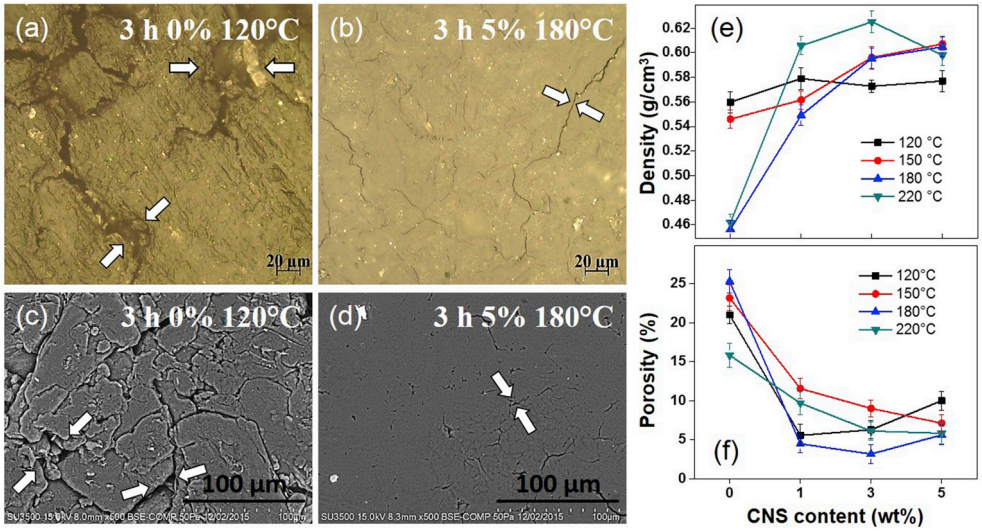

Fig. 6. Micrographs of chitosan samples sintered for 3 h at (a,c) 120 °C with no CNS and (b,d) 180 °C with 5% of CNS. (e) Density and (f) porosity as a function of CNS content and sintering temperature.

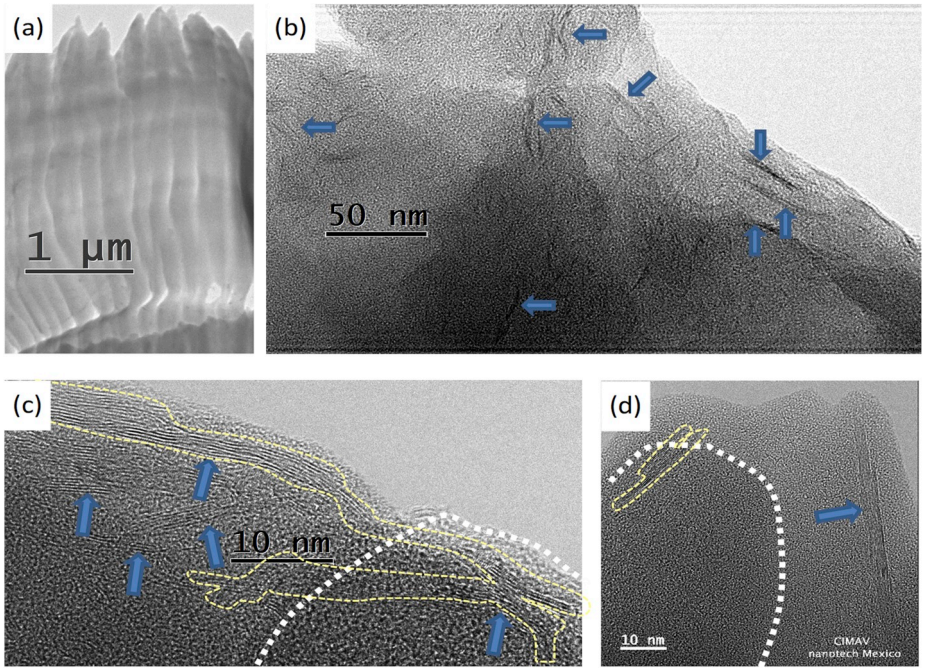

Fig. 7. TEM micrographs of a chitosan/5 wt% CNS sample sintered at 180 °C for 3 h.

stress relief) state of the heavily deformed chitosan particles. Similar effect is seen for higher sintering temperatures, but with shorter times. However, temperatures above 220 °C are detrimental for chitosan integrity's (see Fig. 3a). The XRD results allow to conclude that the sintering at 180 °C for 3 h shows no degradation of the crystalline structure of chitosan, suggesting that this condition is below the degradation threshold, which will prevent chitosan damage.

3.5. Optical and scanning electron microscopies

Fig. 6 shows optical (a,b) and backscattered scanning electron (c,d) micrographs of chitosan and the composites, respectively. In Fig. 6e we show the positive effects of the morphed graphene addition and the sintering temperature increment on the integrity improvement of chitosan, which is translated in the density increment. A density and porosity comparison for the composites and pure chitosan samples is given below. According to the rule of mixtures [36,37] the theoretical increment in density for chitosan with the reinforcement additions is from 1 to 10%. This increment is comparable to that observed in the composites sintered at temperatures of 120 and 150 °C. This is attributed to the clear reduction in porosity in all composites. The case of the composite sintered at 180 °C is explained in more detail below.

It is important to mention that the porosity (Fig. 6f) in the composite sintered at 180 °C shows improvements n density of 82, 87 and 78% for additions of 1, 3 and 5 wt% respectively. Those improvements are unique and as per our recollection we have not seen such benefits in previous reports. We believe that the positive changes shown in Fig. 6e–f are due mainly to the above mentioned anchoring of the chitosan particles by the morphed graphene that it is enhanced by the optimized sintering temperature at 180 °C. Those effects are clearly observed by

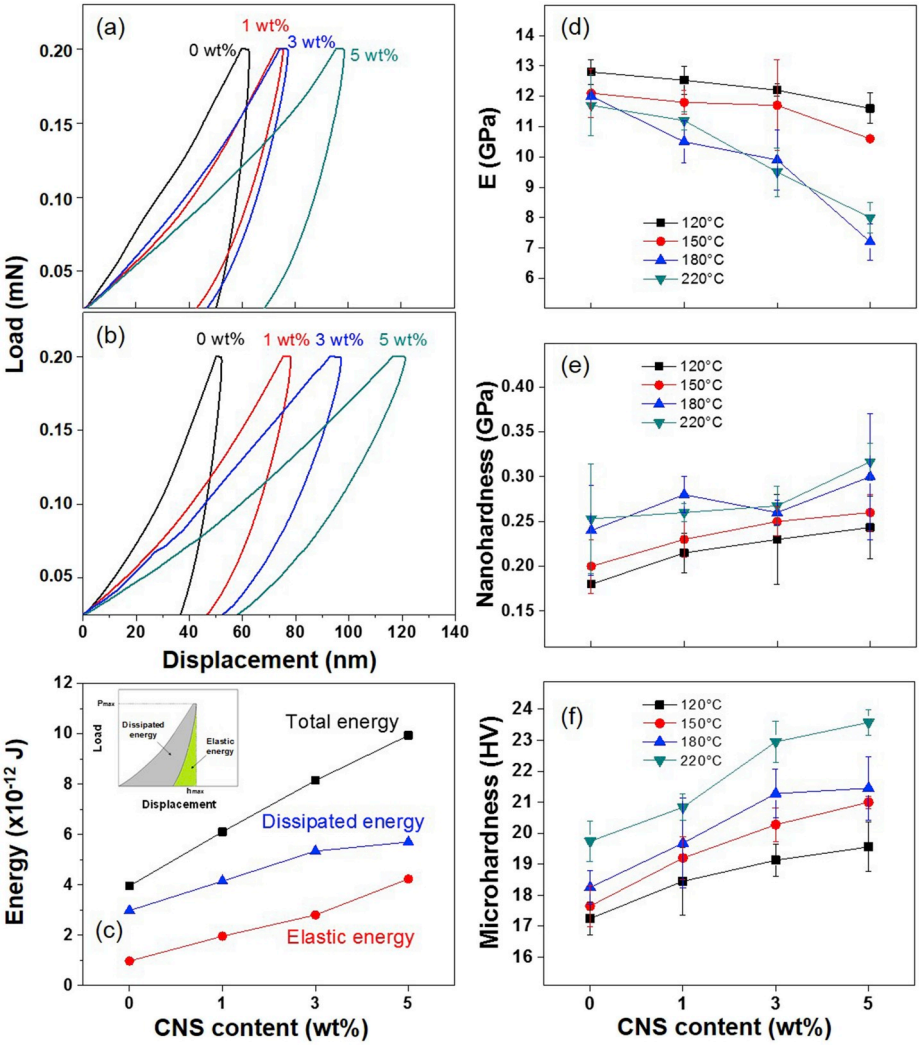

Fig. 8. P-h curves of chitosan samples sintered for 3 h at (a) 120 °C and (b) 180 °C. (c) Elastic, dissipated and applied total energy for deformation during nano-indentation, (d) elastic modulus, (e) nanohardness and (f) microhardness as a function of the CNS content and sintering temperature.

means of optical and scanning electron microscopy (Fig. 6a–d).

3.6. Transmission electron microscopy

Fig. 7 presents bright field TEM micrographs of a raw chitosan particle (Fig. 7a) and HRTEM images of the composites (Fig. 7b–d). In the low-magnification image (Fig. 7b) one can observe the matrix with a large number of morphed graphenes. The morphed graphenes are embedded in the chitosan matrix and in most cases the particles are transgranular among two or more chitosan grains. Selected morphed graphene particles are identified using blue arrows. It is important to notice that some of the morphed graphenes are found along the grain boundaries that is in direct agreement with the Raman results. It means the morphed graphenes are found mainly along the grain's surface of the chitosan particles and as transgranular fibers anchoring the chitosan grains. In the higher-magnification images (Fig. 7c–d) one can see the presence of the morphed graphenes in a transgranular fashion between two or more chitosan grains. An interesting feature to observe in Fig. 7b–d is homogeneity of the composite and good dispersion of the morphed graphenes even at concentration of 5 wt%. It is well known that graphene additions are usually below 1 wt% [38], it is in general accepted that graphene agglomeration is a major limitation in composites when additions are above 3 wt%. However, larger amounts have been reported, but this is only for the dispersion, not in the actual composite [39]. Here we present up to 5 wt% additions of morphe graphenes with rather unique homogeneity in the absence of agglomerations or clusters (Fig. 7). For easy identification, the grain boundary is outlined by thicker dotted (white) lines and the thinner dashed (yellow) lines are used to show the morphed graphenes. This may be perhaps the main mechanism that enables the mechanical improvements in the investigated composites.

3.7. Mechanical properties

The load-displacement (P-h) curves in Fig. 8a and b correspond to samples sintered at 120 °C and 180 °C, respectively. The results are from samples sintered for 3 h, but similar trend was found in samples sintered for 5 h. Control samples (0 wt% CNS) show a low maximum penetration depth for both sintering temperatures, indicating that the material behaves rigid. The maximum penetration depth is higher as the amount of reinforcement increases. For instance, for samples sintered at 180 °C (Fig. 8b), the maximum penetration depth increases from 52 nm for pure chitosan to 78, 97 and 121 nm for composites reinforced with 1, 3 and 5 wt% of morphed graphenes. The resulting improvements are: 50, 87 and 133%, respectively.

The loading portion of the P-h curve (permanent hardness impression occurs) corresponds to the elasto-plastic properties of the material [25]. The unloading portion of the P-h curve represents a pure elastic

behavior, which indicates that all the elastic displacement is recovered after unloading [25]. Thus, it is possible to calculate the energy needed to deform the material both elastically and plastically. Fig. 8c displays the elastic, dissipated and total applied energy of composites sintered at 180 °C, calculated from the areas under the P-h curves of Fig. 8b. All parameters related to the deformation energy of chitosan composites are higher than those of pure chitosan. The elastic energy ratio for chitosan composites shows the following improvements: 30, 40 and 73% for 1, 3 and 5 wt% of morphed graphene, respectively. Therefore, morphed graphene, especially 5 wt%, enhances drastically the elastic performance of chitosan. The complementary improvements (elastic + plastic) reach an approximate 250% improvement. This is a quite important finding as structural materials have always needs for higher toughness.

The improvement in the elastic properties of chitosan with the addition of morphed graphene can be attributed to the elastic characteristics of graphitic particles, in this case morphed graphene. Furthermore, the interfacial bonding between the composite's constituents improves the intimacy and reduce the porosity and grain boundary gaps as demonstrated by optical and scanning electron microscopy (Fig. 6a–d).

Fig. 8d shows how the elastic modulus decreases with sintering temperature and morphed graphene additions. For samples sintered at 180 °C, the decrease represents 12, 18 and 40% for samples with 1, 3 and 5 wt% of morphed graphene, respectively, when compared to pure chitosan. This is in agreement with the results of the elastic energy and the crystallinity index. Fig. 8e shows that the nanohardness increases with the increment of the sintering temperature, as well as with morphed graphene additions. In the case of samples sintered at 180 °C, the nanohardness increases 17, 8 and 25% for composites with 1, 3 and 5 wt% of morphed graphenes, respectively. Here, the temperature effect is attributed to the partial coalescence of the chitosan particles [40]. The nanohardness effects are also observed at the microscale by means of Vickers microhardness (Fig. 8f). The corresponding increments in this case at 180 °C are: 8, 17, and 18% for 1, 3 and 5 wt% of filler additions, respectively. It is evident that the microhardness of the composites increases with sintering temperature due to an improved consolidation. The above results are significant improvements compared to those previously reported [13,41].

The relative higher standard deviation in the nanohardness and moduli measurements when compared to those of microhardness is attributed to the different resolution in both techniques. The microhardness is more of a bulk technique, particularly for nanostructured materials, while nanohardness measurements can be affected by the presence of grain boundaries, morphed graphene and pure chitosan. Therefore, this is an expected result for the nature of the material and the used techniques.

4. Conclusions

Here we present the results of the chitosan composites reinforced with morphed graphenes. The main contributors to the outstanding improvements in mechanical properties are the morphed graphenes, milling processing and sintering temperature. The main improvements are identified in density, porosity, hardness, moduli, toughness, and elastic limit, among others. In summary, the best results are for the composite reinforced with 5 wt% of reinforcement sintered at 180 °C, in comparison to pure chitosan. The major improvements are: density increment 33%, porosity reduction 78%, nanohardness 25%, microhardness 18%, and total toughness (elastic + plastic) in 250%. In terms of density, we can explain relatively easy the increase due to the introduction of the reinforcement. Yet, the porosity reduction is unique and potentially never reported before as a filler contribution. It is where our filler (morphed graphene), processing methods and sintering conditions play an ultimate goal on material's integrity. The main reason for those improvements is the high homogeneity along with the intercalation of the filler taking place during milling. The filler is mainly found in transgranular and intergranular fashions. Results demonstrate that the incorporation of morphed graphenes in chitosan produces a tougher biopolymer, which broaden its bio-degradable potential moving the chitosan composites a step ahead.

Acknowledgements

This work was supported by Department of Mechanical Engineering Technology at University of Houston and Centro de Investigacion en Materiales Avanzados. OVM thanks CONACYT for their scholarship (grant 659774). JMHR is grateful with CONACYT for the support given during his sabbatical stay (grant 255695). HAC acknowledges support from IPN, Mexico (EDI) and COFAA, Mexico. Work at the Molecular Foundry was supported by the Office of Science, Office of Basic Energy Sciences, of the U.S. Department of Energy under Contract No. DE-AC02-05CH11231. Thanks are due to D. Lardizabal-Gutiérrez, L. de la Torre-Saenz, R. Castaneda-Balderas and R.P. Talamantes-Soto for their laboratory assistance.

Appendix A. Supplementary data

Supplementary data to this article can be found online at https://doi.org/10.1016/j.compscitech.2019.107836.

References

[1] M.F. Goosen, Applications of Chitan and Chitosan, CRC Press, 1996.
[2] L.-M. Zhao, L.-E. Shi, Z.-L. Zhang, J.-M. Chen, D.-D. Shi, J. Yang, Z.-X. Tang, Preparation and application of chitosan nanoparticles and nanofibers, Braz. J. Chem. Eng. 28 (3) (2011) 353–362.
[3] N.M. Ospina, S.P.O. Alvarez, D.M.E. Sierra, D.F.R. Vahos, P.A.Z. Ocampo, C.P. O. Orozco, Isolation of chitosan from Ganoderma lucidum mushroom for biomedical applications, J. Mater. Sci. Mater. Med. 26 (3) (2015) 135.
[4] S.E. Bailey, T.J. Olin, R.M. Bricka, D.D. Adrian, A review of potentially low-cost sorbents for heavy metals, Water Res. 33 (11) (1999) 2469–2479.
[5] A. Zamani, L. Edebo, B. Sjöström, M.J. Taherzadeh, Extraction and precipitation of chitosan from cell wall of zygomycetes fungi by dilute sulfuric acid, Biomacromolecules 8 (12) (2007) 3786–3790.
[6] H.W. Kroto, J.R. Heath, S.C. O'Brien, R.F. Curl, R.E. Smalley, C60: Buckminsterfullerene, Nature 318 (6042) (1985) 162.
[7] O. Shenderova, V. Zhirnov, D. Brenner, Carbon nanostructures, Crit. Rev. Solid State Mater. Sci. 27 (3–4) (2002) 227–356.
[8] A.K. Geim, K.S. Novoselov, The Rise of Graphene, Nanoscience and Technology: A Collection of Reviews from Nature Journals, World Scientific2010, 2009, pp. 11–19.
[9] S. Iijima, T. Ichihashi, Single-shell carbon nanotubes of 1-nm diameter, Nature 363 (6430) (1993) 603.
[10] H. Calderon, I. Estrada-Guel, F. Alvarez-Ramírez, V. Hadjiev, F.R. Hernandez, Morphed graphene nanostructures: experimental evidence for existence, Carbon 102 (2016) 288–296.
[11] H. Calderon, A. Okonkwo, I. Estrada-Guel, V. Hadjiev, F. Alvarez-Ramírez, F. R. Hernández, HRTEM low dose: the unfold of the morphed graphene, from amorphous carbon to morphed graphenes, Adv. Struct. Chem. Imag. 2 (1) (2017) 10.
[12] H.A. Calderon, F. Alvarez Ramirez, D. Barber, V.G. Hadjiev, A. Okonkwo, R. Ordoñez Olivares, I. Estrada Guel, F.C. Robles Hernandez, Enhanced elastic behavior of all-carbon composites reinforced by in situ synthesized morphed graphene, Carbon 153 (2019) 657–662.
[13] S.-F. Wang, L. Shen, W.-D. Zhang, Y.-J. Tong, Preparation and mechanical properties of chitosan/carbon nanotubes composites, Biomacromolecules 6 (6) (2005) 3067–3072.
[14] N. Badi, A.R. Erra, F.C.R. Hernandez, A.O. Okonkwo, M. Hobosyan, K. S. Martirosyan, Low-cost carbon-silicon nanocomposite anodes for lithium ion batteries, Nanoscale Res. Lett. 9 (1) (2014) 360.
[15] F. Robles Hernández, H. Calderon, Nanostructured Al/Al4C3 composites reinforced with graphite or fullerene and manufactured by mechanical milling and spark plasma sintering, Mater. Chem. Phys. 132 (2–3) (2012) 815–822.
[16] A.E. Fals, V.G. Hadjiev, F.C.R. Hernandez, Multi-functional fullerene soot/alumina composites with improved toughness and electrical conductivity, Mater. Sci. Eng: A 558 (2012) 13–20.
[17] F.C. Robles-Hernández, H. Calderon, Nanostructured metal composites reinforced with fullerenes, JOM (J. Occup. Med.) 62 (2) (2010) 63–68.
[18] V. Garibay-Febles, H. Calderon, F. Robles-Hernández, M. Umemoto, K. Masuyama, J. Cabanas-Moreno, Production and characterization of (Al, Fe)-C (graphite or fullerene) composites prepared by mechanical alloying, Mater. Manuf. Process. 15 (4) (2000) 547–567.
[19] C. Suryanarayana, Mechanical alloying and milling, Prog. Mater. Sci. 46 (1) (2001) 1–184.

[20] B. Sharma, P. Malik, P. Jain, Biopolymer reinforced nanocomposites: a comprehensive review, Mater. Today Commun. 16 (2018) 353–363.
[21] C. Brysch, E. Wold, M. Patterson, R.O. Olivares, J. Eberth, F.R. Hernandez, Chitosan and chitosan composites reinforced with carbon nanostructures, J. Alloy. Comp. 615 (2014) S515–S521.
[22] O. Velazquez-Meraz, A. Tejeda-Ochoa, J. Ledezma-Sillas, C. Carreño-Gallardo, F. Robles-Hernandez, J. Herrera-Ramirez, The effect of fullerene soot on the mechanical properties of chitosan, Microsc. Microanal. 23 (2017) 1352–1353. S1.
[23] W.H. Cubberly, Tool and Manufacturing Engineers Handbook Desk Edition, Society of Manufacturing Engineers, 1989.
[24] B. Focher, P. Beltrame, A. Naggi, G. Torri, Alkaline N-deacetylation of chitin enhanced by flash treatments. Reaction kinetics and structure modifications, Carbohydr. Polym. 12 (4) (1990) 405–418.
[25] W.C. Oliver, G.M. Pharr, An improved technique for determining hardness and elastic modulus using load and displacement sensing indentation experiments, J. Mater. Res. 7 (6) (1992) 1564–1583.
[26] N. Kikuchi, M. Kitagawa, A. Sato, E. Kusano, H. Nanto, A. Kinbara, Elastic and plastic energies in sputtered multilayered Ti–TiN films estimated by nanoindentation, Surf. Coat. Technol. 126 (2–3) (2000) 131–135.
[27] I. Olivas-Armendáriz, P. García-Casillas, A. Martel-Estrada, R. Martinez-Sánchez, A. Martínez-Villafañe, C.A. Martínez-Pérez, Preparación y caracterización de compositos de quitosana/nanotubos de carbono, Revista mexicana de ingeniería química 8 (2009) 205–211.
[28] M. Ziegler-Borowska, D. Chełminiak, H. Kaczmarek, A. Kaczmarek-Kędziera, Effect of side substituents on thermal stability of the modified chitosan and its nanocomposites with magnetite, J. Therm. Anal. Calorim. 124 (3) (2016) 1267–1280.
[29] I. Mochida, M. Egashira, H. Koura, D.-H. Jung, S.-H. Yoon, Y. Korai, F. Kasuga, J. J. Crelling, The Characterization and Utilization of Fullerene Soot, 22nd Biennial Conference of the American Carbon Society, University of California, San Diego, CA, 1995. July 16-21.
[30] H.S. Mansur, A.A. Mansur, E. Curti, M.V. De Almeida, Functionalized-chitosan/quantum dot nano-hybrids for nanomedicine applications: towards biolabeling and biosorbing phosphate metabolites, J. Mater. Chem. B 1 (12) (2013) 1696–1711.
[31] D. de Britto, S.P. Campana-Filho, Kinetics of the thermal degradation of chitosan, Thermochim. Acta 465 (1–2) (2007) 73–82.
[32] W. Feng, Y. Li, P. Ji, Interaction of water soluble chitosan with multiwalled carbon nanotubes, AIChE J. 58 (1) (2012) 285–291.
[33] M.K. Jang, B.G. Kong, Y.I. Jeong, C.H. Lee, J.W. Nah, Physicochemical characterization of α-chitin, β-chitin, and γ-chitin separated from natural resources, J. Polym. Sci. A Polym. Chem. 42 (14) (2004) 3423–3432.
[34] E. Leonel, E. Nassar, K. Ciuffi, M. dos Reis, P. Calefi, Effect of high-energy ball milling in the structural and textural properties of kaolinite, Cerâmica 60 (354) (2014) 267–272.
[35] Z. Cai, P. Chen, H. Jin, J. Kim, The effect of chitosan content on the crystallinity, thermal stability, and mechanical properties of bacterial cellulose—chitosan composites, Proc. Inst. Mech. Eng. C J. Mech. Eng. Sci. 223 (10) (2009) 2225–2230.
[36] H.S. Kim, On the rule of mixtures for the hardness of particle reinforced composites, Mater. Sci. Eng: A 289 (1) (2000) 30–33.
[37] G. Liu, A step-by-step method of rule-of-mixture of fiber-and particle-reinforced composite materials, Compos. Struct. 40 (3–4) (1997) 313–322.
[38] P. May, U. Khan, A. O'Neill, J.N. Coleman, Approaching the theoretical limit for reinforcing polymers with graphene, J. Mater. Chem. 22 (4) (2012) 1278–1282.
[39] D.W. Johnson, B.P. Dobson, K.S. Coleman, A manufacturing perspective on graphene dispersions, Curr. Opin. Colloid Interface Sci. 20 (5) (2015) 367–382.
[40] C. Wang, X. Zhou, M. Wang, Influence of sintering temperatures on hardness and Young's modulus of tricalcium phosphate bioceramic by nanoindentation technique, Mater. Char. 52 (4–5) (2004) 301–307.
[41] M.Z. Albanna, T.H. Bou-Akl, H.L. Walters III, H.W. Matthew, Improving the mechanical properties of chitosan-based heart valve scaffolds using chitosan fibers, J. Mech. Behav. Biomed. Mater. 5 (1) (2012) 171–180.